Correlating preclinical animal studies and human clinical trials of a multifunctional, polymeric nanoparticle

Scott Eliasof[a], Douglas Lazarus[a], Christian G. Peters[a], Roy I. Case[a], Roderic O. Cole[a], Jungyeon Hwang[a], Thomas Schluep[b], Joseph Chao[c], James Lin[c], Yun Yen[c], Han Han[d], Devin T. Wiley[d], Jonathan E. Zuckerman[d], and Mark E. Davis[d,1]

[a]Cerulean Pharma, Cambridge, MA 02139; [b]Calando Pharmaceuticals, Pasadena, CA 91101; [c]City of Hope Comprehensive Cancer Center, Duarte, CA 91010; and [d]Chemical Engineering, California Institute of Technology, Pasadena, CA 91125

Edited* by Joseph M. DeSimone, The University of North Carolina at Chapel Hill, Chapel Hill, NC, and approved July 30, 2013 (received for review May 20, 2013)

Nanoparticles are currently being investigated in a number of human clinical trials. As information on how nanoparticles function in humans is difficult to obtain, animal studies that can be correlative to human behavior are needed to provide guidance for human clinical trials. Here, we report correlative studies on animals and humans for CRLX101, a 20- to 30-nm-diameter, multifunctional, polymeric nanoparticle containing camptothecin (CPT). CRLX101 is currently in phase 2 clinical trials, and human data from several of the clinical investigations are compared with results from multispecies animal studies. The pharmacokinetics of polymer-conjugated CPT (indicative of the CRLX101 nanoparticles) in mice, rats, dogs, and humans reveal that the area under the curve scales linearly with milligrams of CPT per square meter for all species. Plasma concentrations of unconjugated CPT released from CRLX101 in animals and humans are consistent with each other after accounting for differences in serum albumin binding of CPT. Urinary excretion of polymer-conjugated CPT occurs primarily within the initial 24 h after dosing in animals and humans. The urinary excretion dynamics of polymer-conjugated and unconjugated CPT appear similar between animals and humans. CRLX101 accumulates into solid tumors and releases CPT over a period of several days to give inhibition of its target in animal xenograft models of cancer and in the tumors of humans. Taken in total, the evidence provided from animal models on the CRLX101 mechanism of action suggests that the behavior of CRLX101 in animals is translatable to humans.

nanomedicine | clinical translation | interspecies scaling | pharmacodynamics | Nanoparticles

Multifunctional nanoparticles are emerging as a new class of therapeutic agents (1). Several types of nanoscaled therapeutic agents such as PEGylated proteins, albumin-based formulations, polymeric micelles, and liposomes are already approved for human use, and these so-called "first-generation" (2) nanoscaled therapeutic agents have provided a basis for the design of newer multifunctional nanoparticles (1–3). A small number of multifunctional nanoparticles have been translated into clinical studies (4–9). These nanoparticles are less than 100 nm in diameter and carry payloads such as small-molecule drugs, e.g., camptothecin (CPT) (7), docetaxel (8), or siRNA (9). A few of these nanoparticles also contain targeting ligands (8, 9) that aid in their internalization into tumor cells. Some of the issues with the use of targeting ligands such as added cost and complexity have recently been described (10). These designed, multifunctional nanoparticles are revealing interesting behaviors in early clinical trials, e.g., they can significantly reduce side effects of the therapeutic molecules they carry, and they do not show new side effects as a result of the nanoparticle.

Polymeric nanoparticles [as opposed to polymer–drug conjugates (1)] are currently undergoing clinical investigation for the treatment of cancer (4–9, 11) and for use as vaccines (4, 5). These clinical studies are providing initial information on the behavior of sub–100-nm polymeric nanoparticles in humans. For example, Davis et al. demonstrated that the amount of nanoparticles localized in melanoma tumors could be correlated to the amount of the systemic dose administered to patients (9). However, data on how nanoparticles function in humans are difficult to obtain. Thus, animal studies are used to provide guidance. One key issue is whether the results from these animal studies correlate with those in humans, i.e., what are the interspecies variations in nanoparticle behavior? Therefore, there is a large need to understand the relationships between the human and animal data, and to determine which behaviors in humans can be reliably predicted from preclinical data with sub–100-nm nanoparticles. Recently, data describing the formulation of BIND-014 and its pharmacokinetic (PK) behavior in animals and humans has been reported (8).

Here, we present translational data from the nanoparticle denoted CRLX101 (formerly called IT-101). This multifunctional nanoparticle is currently being investigated in a number of phase 2 clinical trials for cancer. To our knowledge, CRLX101 was the first de novo designed, polymeric nanoparticle to reach the clinic (12).

CRLX101 is comprised of a cyclodextrin-containing polymer conjugate of CPT (Fig. 1*A*). The cyclodextrin-containing polymer was designed to have very high aqueous solubility with low charge (ζ-potential of CRLX101 is ca. −6 mV in PBS solution), as high charge (especially polycations) can create a number of unwanted effects, including complement activation in mammals. That way, the highly soluble polymer can be conjugated with very low-solubility drugs. The cyclodextrin-containing polymer is conjugated via glycine to the relatively insoluble CPT and increases its effective solubility vs. that of the drug molecule alone by approximately three orders of magnitude (12). The linker chemistry can be tuned to provide a variety of release behaviors. Specifically, the glycine linker used in CRLX101 was chosen to provide slow release of the lactone form (the active form) of CPT at acidic conditions that would be experienced when the nanoparticles enter cells (12). The polymer strands self-assemble into a nanoparticle (approximately five strands) of approximately 20 to 30 nm diameter and 10 wt% CPT by multiple, interstrand, inclusion complex formation between cyclodextrin and the CPT molecules (Fig. 1*A*).

CRLX101 has been shown to circulate in rodents with a $t_{1/2}$ of approximately 1 d (13, 14) and accumulate in solid tumor xenografts as an intact nanoparticle (13). Additionally, the CRLX101

Author contributions: S.E., J.H., T.S., J.C., Y.Y., D.T.W., J.E.Z., and M.E.D. designed research; D.L., C.G.P., R.I.C., R.O.C., J.H., T.S., J.L., H.H., D.T.W., and J.E.Z. performed research; S.E., J.H., T.S., J.C., J.L., Y.Y., D.T.W., J.E.Z., and M.E.D. analyzed data; and S.E., D.T.W., J.E.Z., and M.E.D. wrote the paper.

Conflict of interest statement: M.E.D. is a consultant to Cerulean Pharma and owns stock in the company.

*This Direct Submission article had a prearranged editor.

Freely available online through the PNAS open access option.

[1]To whom correspondence should be addressed. E-mail: mdavis@cheme.caltech.edu.

This article contains supporting information online at www.pnas.org/lookup/suppl/doi:10.1073/pnas.1309566110/-/DCSupplemental.

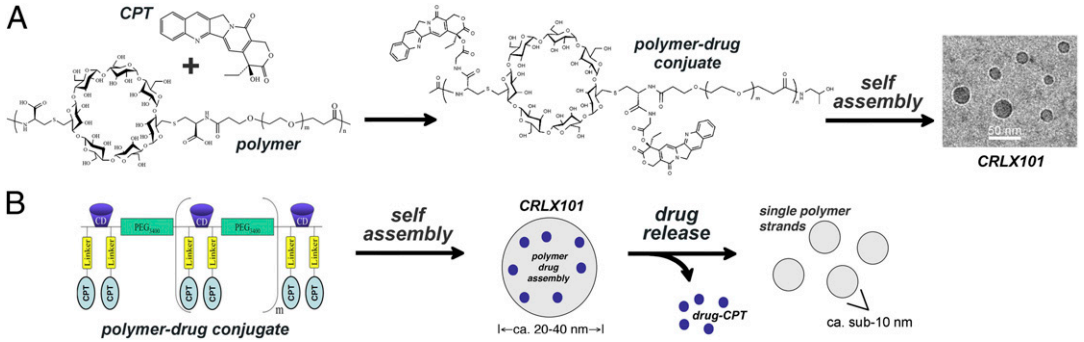

Fig. 1. Schematic diagrams of the assembly and disassembly of CRLX101. (*A*) Schematic of the cyclodextrin-containing polymer conjugate of CPT and its components. (*Right*) Cryo-TEM of the CRLX101 nanoparticles formed by self-assembly of the polymer–drug conjugates. (*B*) Schematic of CRLX101 assembly and disassembly (when the CPT is released).

nanoparticles have been observed [by transmission EM (TEM) images] to localize into cancer cells in a mouse xenograft from a tail vein injection (15). CRLX101 slowly releases the CPT when inside cells to allow for long tumor exposures of the drug, and has been observed to do so over several days in mouse xenografts (16). Released, active CPT from CRLX101 has resulted in indications of prolonged topoisomerase I and HIF-1α inhibition (targets of CPT) in mouse xenografts (15, 16), and has provided increased antitumor activity compared with irinotecan and topotecan (both are Food and Drug Administration-approved analogues of CPT) (12, 15–17). The CRLX101 nanoparticle is designed to disassemble when the CPT is released to give individual polymer strands that are synthesized to have molecular weights sufficiently small to allow for clearance via the kidney (Fig. 1*B*) (12, 13).

Herein, we present results from phase 1a, 1b, and 2a (7) clinical trials and correlate them to animal data to elucidate how the multifunctional behavior of CRLX101 translates from animals to humans.

Results

Preclinical and Clinical Lots of CRLX101 Give 20- to 30-nm-Diameter Nanoparticles. The synthesis and properties of preclinical nanoparticles of CRLX101 have been described previously (12–18). The nanoparticles were 20 to 30 nm in diameter, and characterization studies demonstrated that all the polymer chains were contained within the nanoparticles (i.e., no free polymer chains) (13). A schematic of the process for the synthesis and formulation of CRLX101 into vials is provided in *SI Appendix*, Fig. S1. Various lots of CRLX101 were prepared and used in clinical studies. A summary of some of these lots and their properties is given in *SI Appendix*, Table S1. Similar to the preclinical versions of CRLX101, clinical lots A, B, and E tested negative for the presence of free polymer chains.

Because the nanoparticles are composed of organic material and are quite small, measurements of size via dynamic light scattering (DLS) can be difficult. To verify sizes measured by DLS and determine accurate size distributions, several lots were imaged by using cryo-TEM. A representative image and the size distributions for two lots are provided in *SI Appendix*, Figs. S2–S5. In general, there is good agreement between the DLS nanoparticle sizes and those measured by cryo-TEM (*SI Appendix*, Table S1 and Figs. S3–S5). Also, the mean value of the size and the size distributions by DLS or cryo-TEM vary only slightly from lot to lot (*SI Appendix*, Table S1 and Figs. S3–S5).

Human Plasma PK Shows Long Circulation of the Nanoparticles and Areas Under the Curve of Polymer Conjugated CPT Scale Linearly with Dose. CLRX101 was administered to patients as 60- to 90-min infusions (7). Fig. 2*A* shows the mean plasma concentrations of the payload CPT that is conjugated to the polymer of CRLX101 and CPT that is not conjugated to the polymer (i.e., was released from the polymer) for several dose levels from the phase 1a clinical trial. For the conjugated CPT, the maximum concentration is observed within 2 h of ending the infusion, whereas the maximum concentration of the unconjugated CPT occurs at a much later time. A summary of the PK data is listed in *SI Appendix*, Table S2. The patient-to-patient variations in the PK parameters at any given dose level are small (7), and the area under the curve (AUC) for the conjugated or unconjugated CPT increases in a linear fashion with the dose in milligrams of CPT per square meter (Fig. 2*B*).

Animal and Human AUCs Scale Linearly with Dose. Fig. 3 illustrates the striking similarity of PK parameters obtained from rats and dogs (Fig. 3 *A* and *B*) and humans (Fig. 3*C*) for the conjugated CPT. Fig. 3*D* shows data that demonstrate that the AUC of the polymer-conjugated CPT scales linearly with milligrams of CPT per square meter, and that the results from animals and humans follow the same relationship.

Animal and Human PK Parameters Are Unchanged upon Repeat Dosing. The data displayed in Fig. 3 *A*–*C* show that, after repeat dosing, there are no appreciable changes in the PK for the polymer-bound and unconjugated CPT in any of the animal or human studies. Human PK parameters were measured for conjugated and unconjugated CPT after the first dose of CRLX101 to the patient and after the first dose of the sixth monthly cycle, i.e., the eleventh dose of CRLX101. No statistically significant differences are observed between the PK parameters from repeat dosing (*SI Appendix*, Table S3), and no intrapatient changes are observed in AUC or clearance (*SI Appendix*, Fig. S6).

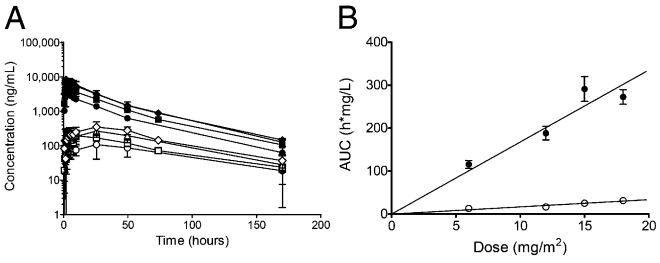

Fig. 2. Human plasma PK parameters. (*A*) Plasma concentrations of conjugated CPT (closed symbols) and unconjugated CPT (open symbols) as a function of time from the phase 1a clinical trial. Data points represent mean, and error bars represent SD (n = 6 per dose level). Circles, 6 mg/m^2; squares, 12 mg/m^2; triangles, 15 mg/m^2; diamonds, 18 mg/m^2. (*B*) AUC as a function of dose level for conjugated CPT (closed symbols) and unconjugated CPT (open symbols). Data points represent mean, and error bars represent SD (n = 6 per data point). CRLX101 lots A and E were used in this study.

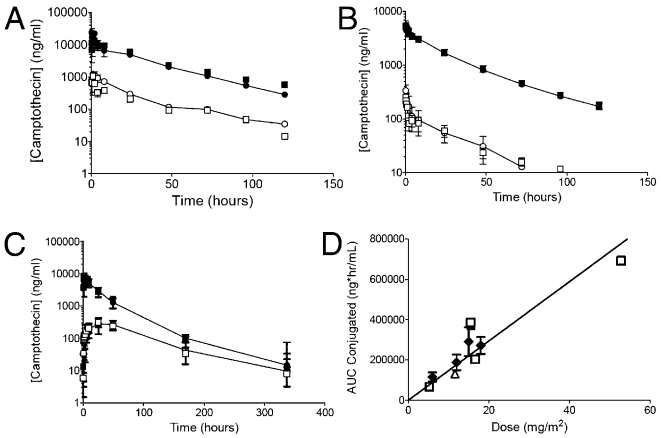

Fig. 3. Interspecies CRLX101 PK comparison. (*A* and *B*) Plasma concentrations of conjugated CPT (closed symbols) and unconjugated CPT (open symbols) as a function of time in rats (*A*) and dogs (*B*). Circles represent first dose, and squares represent third weekly dose. Data points represent mean, and error bars represent SD ($n = 6$ per data point). (*C*) Plasma concentrations of conjugated CPT (closed symbols) and unconjugated CPT (open symbols) as a function of time from the phase 2a clinical trial. Circles represent first dose, and squares represent 11th biweekly dose (cycle 6, day 1). Data points represent mean, and error bars represent SD. (*D*) AUC as a function of dose level across species for conjugated CPT. The line is a linear regression against all data points ($R^2 = 0.802$). Data points represent mean, and error bars represent SD ($n = 6$ per data point). Squares, rat; triangles, dog; diamonds, human. Closed symbols, male; open symbols, female.

PK of Unconjugated CPT Depends on Its Binding to Serum Albumin. The time-dependent behavior of the conjugated CPT appears similar between animals and humans (Fig. 3 *A*–*C*). However, this is not the case for the unconjugated CPT. The dynamics in the human are not what are observed in the various animals models (the interspecies animal data are consistent). To provide a plausible explanation for these data, the dynamics of the conjugated and unconjugated CPT were modeled (*SI Appendix*, *Supplementary Materials and Methods*). The simulations (*SI Appendix*, Figs. S7 and S8) are able to recapitulate the experimental observations, and suggest that the differences in the human dynamics of unconjugated CPT result from the high binding affinity between human albumin and CPT [CPT binds with higher affinity to human albumin than albumin from other species (19)]. After taking into account these interspecies variations in albumin binding, the unconjugated CPT PK in humans can be correlated with the preclinical animal data.

PK Is Influenced by Nanoparticle Drug Loading but Not Polymer Molecular Weight. Polymer molecular weight and drug loading are two key parameters that are controlled and measured during the formulation of CRLX101. To understand how these nanoparticle properties correlate with PK, the polymer molecular weight and drug loading of several nanoparticles were varied to give high and low bounds for investigation. The PK of these nanoparticles were measured in rats, and the results are listed in *SI Appendix*, Table S4. The rat PK data suggest that a 50% reduction in drug loading accelerates the release of CPT from the nanoparticles, as reflected by increases in the AUC of unconjugated CPT. This result is consistent with the important role that the cyclodextrin–CPT inclusion complex plays in stabilizing CRLX101. With increasing CPT conjugated to the polymer, the nanoparticles are more highly stabilized by a larger number of inclusion complexes. In contrast, changes in polymer molecular weight (over the range investigated) had minimal effects on PK.

The manufacturing process of CRLX101 for clinical use is remarkably consistent, and polymer molecular weight and drug loading do not appreciable vary from lot to lot (*SI Appendix*, Table S1). Although several different lots of CRLX101 were administered to patients over the course of the phase 1 and 2a clinical trials, minimal impact of lot variations on PK was observed. *SI Appendix*, Table S5, lists PK data from patients who received two different lots of CRLX101 in the phase 2a trial.

CPT (Nanoparticle Drug Payload) Release from CRLX101 Is Not via Esterase Activity. The CPT in CRLX101 is conjugated to the polymer via an ester bond (Fig. 1*A*), and, when this bond is cleaved, CPT is released. When a critical number of the CPT molecules are removed from the polymer chain, that chain can be lost from the nanoparticle (nanoparticle disassembly; Fig. 1*B*). To ascertain whether esterase activity could contribute to the release of CPT, the in vitro release kinetics were measured. In all cases, the release kinetics were fit to a first-order process. The $t_{1/2}$ values for CPT release in mouse serum that was freshly collected or frozen at some point were 51 and 49 h, respectively. Thus, the freezing of serum has no effect on the release kinetics. The $t_{1/2}$ that was measured from human serum that had been frozen was 26 h.

Mouse serum has more esterases than human serum (20). As the release of CPT from CRLX101 is faster in human serum than mouse serum, these results suggest that esterase activity is not the main pathway for CPT release. To further this idea, CRLX101 was tested in vitro in the presence of just butyrylcholinesterase (BCHE) in PBS solution because it is contained in mouse and human serum (20). The release $t_{1/2}$ of the CPT was not significantly different in the absence or presence of BCHE. If LDL is added at an amount of 3 mg/mL into PBS solution, the $t_{1/2}$ is 35 h (greater than 100 h in PBS solution alone), and is the same in the presence and absence of BCHE. Taken together, these data suggest that the release of CPT is through the hydrolysis of the ester bond (independent of enzyme activity), and that the presence of lipoprotein complexes like LDL can assist in the disassembly of CRLX101. If the release kinetics of CPT are the result of hydrolysis rates, they should be a function of pH. The release kinetics of CPT from CRLX101 have been shown to be pH-dependent, with longer $t_{1/2}$ values being observed for lower pH values (18). These data suggest that differences in interspecies CPT release kinetics are caused by differences in plasma contents, such as lipoprotein complexes, as opposed to levels of plasma esterases.

CPT and Polymer Conjugated CPT Are Excreted into the Urine. Within the first 8 h after infusion, greater than 10% of the administered dose of CRLX101 was excreted into the urine as conjugated CPT (7). Interestingly, the percentage of the dose excreted declines with increasing dose (7), raising the possibility that the renal excretion processes become saturated. Data provided in Fig. 4 show that the excretion of conjugated CPT reaches a maximum at 15 mg/m^2.

Patients dosed with more than one lot of CRLX101 during their course of treatment did not show significant differences in the amount of CPT excreted (*SI Appendix*, Fig. S9). Analyses of the polymer molecular weight from polymer collected from the patient's urine revealed that the molecular weight distribution was not statistically different from that of the CRLX101 that was administered.

CRLX101 Accumulates in and Penetrates Through Tumors to Release Functional CPT. Some important characteristics of nanoparticles include their ability to prolong drug plasma $t_{1/2}$, to penetrate into tumors via the leaky tumor neovasculature, and to accumulate in tumors as a result of the enhanced permeation and retention effect. In order for these nanoparticle characteristics to translate to superior efficacy, however, it is also beneficial for the nanoparticle to penetrate deep into tumors to kill tumor cells localized far from the vasculature.

By using the intrinsic fluorescence of the CPT component of CRLX101, Fig. 5 *A* and *B* shows images that illustrate that

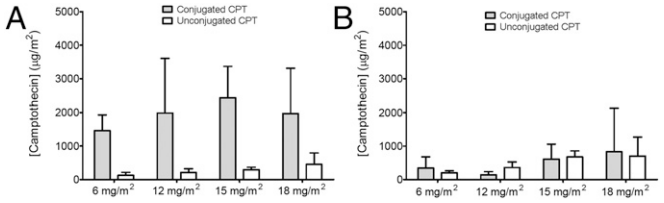

Fig. 4. Urinary excretion of conjugated and unconjugated CPT as a function of dose level. Collection periods are 0 to 24 h (*A*) and 24 to 48 h (*B*). Total drug content was measured and normalized to the body surface area for each patient. Shaded bars represent conjugated CPT, and open bars represent unconjugated CPT. Data points represent mean, and error bars represent SD.

CRLX101 begins to enter tumors of mouse xenografts within 6 h after dosing, and remains in the tumors over several days while diffusing away from the tumor vasculature. By using an anti-PEG antibody, we confirm that CRLX101 deposits in tumors as assembled nanoparticles by showing that CPT and polymer components of CRLX101 are colocalized in tumors (Fig. 5*C*). Once in tumors, the drug payload CPT is released slowly from CRLX101, and can significantly inhibit topoisomerase-1 for as long as 1 wk after a single, submaximal dose (Fig. 5*D*). HIF-1α is also inhibited in this study (*SI Appendix*, Fig. S12), consistent with previously published data (15).

Fig. 5*E* shows an image of CPT signal detected in a tumor biopsy sample taken from a patient with gastric adenocarcinoma 48 h after CRLX101 treatment. The pattern of CPT fluorescence observed in this biopsy specimen is consistent with that seen in the animal models, suggesting that the CPT signal detected with this patient's tumor is from intact CRLX101.

Discussion

CRLX101 is a polymer-based nanoparticle of designed size and ζ-potential. The diameter of approximately 20 to 30 nm allows for movement through solid tumors (13, 21) and the slightly negative ζ-potential at this size helps to minimize uptake by the mononuclear phagocyte system (22). CRLX101 is designed to have high solubility, to circulate and extravasate into solid tumors via their leaky vascular as an intact nanoparticle (13, 15), to enter cancer cells, and to slowly release the active form of CPT for extended periods of time to enhance its mechanism of action (16). The polymer component of CRLX101 is synthesized to be small enough to clear the body via renal excretion after the nanoparticle disassembles into individual polymer strands (Fig. 1*B*).

There are numerous data from animals that support the conclusion that CRLX101 remains as intact nanoparticles in circulation. PET studies of CRLX101 show that polymer-conjugated CPT has a $t_{1/2}$ of approximately 24 h in mice, and that the measured tumor permeability data are consistent with an approximately 30-nm nanoparticle and not an individual polymer strand (13). Additionally, PET-labeled single polymer strands cleared from mice via urinary excretion in less than 1 h. Imaging of mouse tumors indicates that CRLX101 does reach tumors intact (13), and high-resolution TEM images reveal direct visual evidence for intact nanoparticles within tumor cells (15). Thus, we will refer to the polymer-conjugated CPT as the nanoparticle CRLX101.

The PK of CRLX101 in humans (Fig. 2*A*) revealed excellent reproducibility from patient to patient (7). Additionally, the AUC of the polymer-conjugated and unconjugated CPT increased in a linear, dose-dependent manner (Figs. 2*B* and 3*D*). The long circulation of CRLX101 provides extended time for the nanoparticles to extravasate into solid tumors via their leaky vasculature (13). The circulation time in humans was such that patients receiving weekly doses of CRLX101 in the phase 1 clinical trial were experiencing "carryover" of CPT from previous dosing (7). To eliminate the carryover, the administrations were altered to dosing on a biweekly schedule. Patients receiving CRLX101 doses of 15 mg CPT/m^2 on the biweekly schedule showed no polymer-conjugated CPT at 14 d after administration, and, for the unconjugated CPT, they had only 3.1% remaining of the mean maximum concentration (C_{max}) values (7). This dosing amount and schedule is being used for all phase 2 clinical trials.

In the phase 1 and 2a clinical trials of CRLX101, biweekly dosing appears to be well tolerated, no incremental toxicities were observed with long-term (>6 mo) treatment, and the polymer does not appear to contribute to toxicity (7). As shown in the data provided in Fig. 3 and *SI Appendix*, Table S3, there were no effects of treatment cycle on the PK parameters in humans and animals. Thus, it is expected that clearing antibody formation to CRLX101 is not occurring to any significant amount. These results show that the multicycle animal data are predictive of the multicycle data observed in humans. In contrast, PEGylated liposomes have produced hypersensitivity reactions, complement activation, and other side effects that are not observed from the drug alone (23, 24). Additionally, cycle-dependent PK parameters have been observed for PEGylated doxorubicin in humans (i.e., the clearance decreased over three cycles of treatment) (25). Factors influencing the intrapatient and interpatient PK parameters with liposomes are discussed elsewhere (26, 27).

CRLX101 PK results from several animal studies and the clinical data from humans demonstrate that the AUC is linear with dose on the basis of milligrams of CPT per square meter (Fig. 3*D*). These data suggest that interspecies scaling can be done on body surface area. This conclusion is important, as there have not been data available to assess what the proper interspecies scaling should be for polymer-based nanoparticles. Other nanoparticles have shown this type of scaling in humans. For example, Hamaguchi et al. reported from their phase 1 study that the AUC of the polymeric micelle NK105 increases linearly with dose in milligrams per square meter (28). Likewise, Lim et al. reported that the AUC for the polymeric micelle Genexol-PM increases linearly with dose in milligrams per square meter (29). However, we are not aware of data like those displayed in Fig. 3*D* that show the scaling between animals and humans is the same when based on milligrams of CPT per square meter.

The human PK dynamics of unconjugated CPT are not consistent with the animal species amounts and dynamics. We have modeled these dynamics (*SI Appendix*, *Supplementary Materials and Methods*), and the results suggest the different human dynamics are mainly attributable to the much higher binding affinity of CPT to human albumin than the albumin in other species (19). This high binding to human albumin is not observed with the active metabolic of irinotecan, SN-38 (30, 31). When CPT was conjugated to linear PEG, the PK profiles of the released CPT in animals (32) and humans (33, 34) showed the same form of the dynamics as observed for CRLX101. Likewise, the MAG-CPT gave released CPT dynamics of the same type (35, 36). However, the polymeric micelle of SN-38 shows the same behavior for released SN-38 in animals (37) and humans (28), as does PEG-bound SN-38 in animals (38) and humans (39). When CPT binding to albumin is properly accounted for, the PK parameters of the unconjugated CPT in animals and humans can be correlated.

A major issue in the translation of nanoparticle therapeutic agents is that of how lot-to-lot (i.e., preparation-to-preparation) variations affect performance. Initially, the PK parameters in rats were investigated as a function of polymer molecular weight and drug loading, as these parameters are critical to the formulation and performance of CRLX101. High and low values for polymer molecular weight and CPT loading were chosen to define a parameter space larger than expected from the lot-to-lot variations in clinical-grade CRLX101. These parameters and the resulting PK data obtained in rats are given in *SI Appendix*, Table S4. There were no appreciable differences in the rat PK parameters

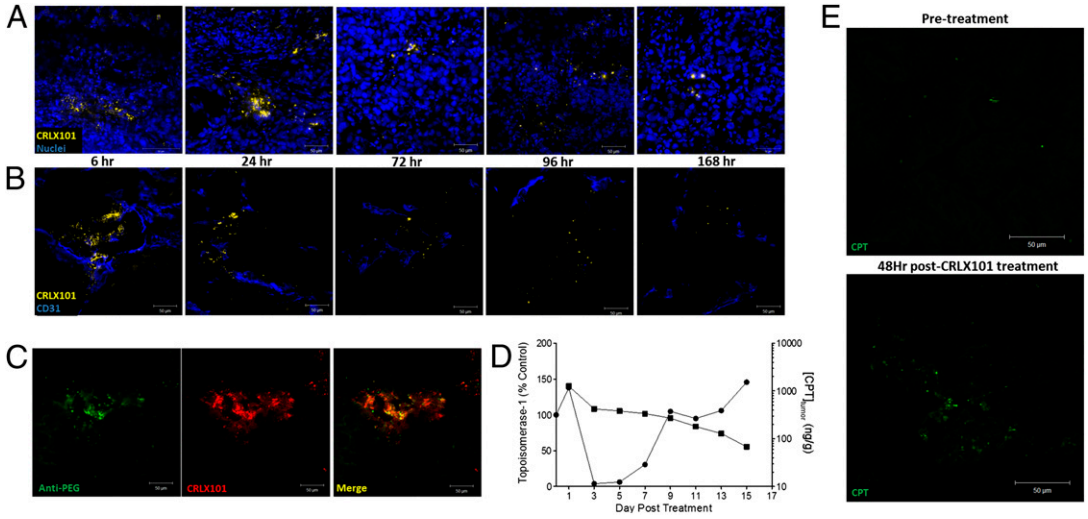

Fig. 5. CPT in tumors of mice and humans. (*A* and *B*) Fluorescence microscopy demonstrates tumor penetration of CRLX101 over 1 wk following a single dose in NCI-H2122 KRAS mutant non–small-cell lung cancer xenografts. Yellow color is CPT fluorescence (*SI Appendix*, Fig. S10, shows excitation spectrum), and blue color is (*A*) nuclei or (*B*) blood vessels stained with anti-CD31. CPT fluorescence is maximal at 24 h and still detectable at diminished levels at 168 h. CPT fluorescence is more tightly associated with blood vessels at earlier time points. (*C*) Fluorescence microscopy demonstrates polymer (anti-PEG antibody) and CPT fluorescence colocalization, suggesting that CPT fluorescence signal in the tumor comes from intact CRLX101 nanoparticles. (*D*) Prolonged tumor exposure to CPT correlates with prolonged inhibition of topoisomerase-1 (*SI Appendix*, Fig. S11). Mice bearing NCI-H1299 non–small-cell lung cancer tumors were dosed once with 6 mg/kg CRLX101, and tumors were harvested and analyzed at the times indicated for CPT concentration (squares) and topoisomerase-1 expression (circles). CPT concentrations were measurable for >2 wk after a single dose, and topoisomerase-1 inhibition was evident for >1 wk, demonstrating sustained release of CPT in tumors. (*E*) Detection of CPT fluorescence in a tumor biopsy sample taken from a patient with gastric adenocarcinoma 48 h after CRLX101 treatment. CPT signal is bright green (punctate green dots) and not observed in the pretreatment tumor biopsy.

when the polymer molecular weight was varied. However, a 50% reduction in CPT loading increased the AUC of unconjugated CPT in rat PK experiments, presumably by destabilizing the nanoparticles and allowing for faster release of CPT. Given this information, the lot-to-lot variations on CPT loading in the clinical CRLX101 samples were kept to a minimum (*SI Appendix*, Table S1). The PK data from humans for two different lots of CRLX101 (*SI Appendix*, Table S5) demonstrate that changes in nanoparticle size and loading in different clinical batches did not result in major differences in the human PK (and also urinary excretion; *SI Appendix*, Fig. S9).

CRLX101 is designed to disassemble when CPT is released from the nanoparticles. Previous studies have shown that CRLX101 drug–polymer conjugate strands are fully incorporated into nanoparticles with no free, low molecular weight conjugate present in the formulation (13). Several clinical lots of CRLX101 were also tested for free polymer conjugate, and none were detected. A prolonged plasma $t_{1/2}$ of CRLX101 facilitated by a nanoparticle size that exceeds the kidney filtration limit of approximately 10 nm suggests that the source of polymer-bound CPT in urine is from individual drug–polymer strands after nanoparticle disassembly. Apparently, disassembly does not require that all the drug molecules be released from each strand. When disassembly has occurred, these partially drug-bound polymer strands are small enough that they would pass rapidly through the kidney. The molecular weight of the polymer that is excreted into the urine is the same as in the dosed CRLX101; therefore, there is no fractionation of the polymer strands by molecular weight in the human. The release of CPT from CRLX101 is via hydrolysis, but serum components appear to be able to interact with the nanoparticles to increase the availability of the CPT for release, and are likely accountable for some of the differences in the release kinetics between animals and humans. In humans, the urinary excretion appears to involve some process that can be saturated. At this time, it is not clear what this process is. However, it is important to point out that no toxicities of the kidney are observed in any of the clinical studies reported thus far (7).

No human biodistribution data are available. However, the biodistribution of CRLX101 has been investigated in animals, and accumulations in kidney, liver, and spleen are observed in addition to tumor (13, 14). In mice, the total amount of CPT per gram of tissue (14) and polymer (that is indicative of CRLX101 nanoparticles) are the highest in the tumor tissue at 24 h after administration (13). Urinary excretion of polymer-conjugated CPT occurs primarily within the initial 24 h after dosing in animals and humans. Given that the PK and urine excretion dynamics in animals and humans are correlated, it is expected that the human biodistribution should be similar to that observed in animals.

The safety profile of CRLX101 at the maximum tolerated dose of 15 mg CPT/m^2 administered biweekly has been reported (7). Overall, CRLX101 is very well tolerated, and the side effects obtained are attributable to the known side effects of CPT. No new side effects of the nanoparticle are observed (7). Thus, it is most likely that the side effects from administering CRLX101 in humans are from the payload and not from the nanoparticle itself.

Accumulation of CRLX101 into mouse tumor xenografts has been investigated previously (13–16), and the time-dependent localization in one tumor type is illustrated in Fig. 5 *A* and *B*. The nanoparticles are shown to move away from tumor vasculature and reside in the tumor for many days. The slow release of CPT has been reported previously (16), and here it is shown that the released CPT can significantly inhibit topoisomerase-1 activity for as long as 1 wk after a single, submaximal dose (Fig. 5*D*). A biopsy of a human gastric adenocarcinoma revealed CPT signal was present 48 h after CRLX101 administration (Fig. 5*E*). The pattern of distribution of CPT signal observed in the human gastric tumor was similar to the pattern of distribution of CRLX101 observed in the mouse xenografts. Additionally, a tumor biopsy from a patient with triple-negative breast cancer receiving CRLX101 dosing of 15 mg CPT/m^2 revealed the presence of CPT 14 d after dosing (7). This long tumor exposure of CPT in humans is consistent with data from previous animal models (16) and those shown in Fig. 5.

Taken in total, the evidence provided from animal models on the CRLX101 mechanism of action suggests that the nanoparticle behavior in animals is translatable to humans. Although there are interspecies differences that need to be accounted for, such as the serum albumin binding of CPT and plasma components that affect the CPT release kinetics, the overall PK and pharmacodynamic parameters from animals and humans do appear to be correlated.

Materials and Methods

Complete details of materials and methods are provided in *SI Appendix, Supplementary Materials and Methods*.

Synthesis of CRLX101 for Rat PK Study. CRLX101 was synthesized by using methods described elsewhere (18).

Cryo-TEM Imaging. Images were collected on a Tecnai 120-keV transmission electron microscope (FEI Company) equipped with a Gatan 2k × 2k UltraScan CCD camera (Gatan).

CRLX101 In Vitro Release Kinetics. Release of CPT from CRLX101 was conducted at 0.32 mg CPT/mL in BALB/c mouse plasma, human plasma, and PBS solution, pH 7.4, in the presence and absence of 100 U/mL of BCHE and/or 3 mg/mL LDL.

Plasma and Urine PK Study in Rat, Dog, and Human. Rats were dosed at 2.59 mg/kg (Fig. 2) or 3 mg/kg CRLX101 (CPT equivalent), and beagle dogs were dosed at 0.58 m/kg CRLX101 (CPT equivalent) by i.v. injection. Patients from the phase 1 and 2a clinical trials were dosed as described previously (7). Patient urine was analyzed for conjugated and released CPT by using methods described elsewhere (7).

Mouse Tumor PK Study. Tumor samples were homogenized in 1:1 DMSO: water, 0.1% formic acid. The homogenates were centrifuged, and the supernatant was collected for processing.

Measurement of Mouse Tumor Topoisomerase-1. At the time points indicated, mice were killed, and tumors were harvested and homogenized for immunoblotting. Immunoblotting was performed by using anti-topoisomerase 1 (1:1,000; Abcam) and anti-actin (1:2,500; Santa Cruz) antibodies. IRDye-conjugated anti-mouse and anti-rabbit secondary antibodies (1:10,000; LI-COR) were visualized on the Odyssey CLx infrared imaging system.

Tumor Penetration. At the time points indicated, mice were killed and the tumors were embedded in optimal cutting temperature compound and frozen. All mice were treated according to the National Institutes of Health Guidelines for Animal Care and Use as approved by the Caltech Institutional Animal Care and Use Committee. Human gastric adenocarcinoma sample was obtained from a patient enrolled in a CRLX101 pilot trial with consent in accordance with City of Hope Institutional Review Board (IRB) guidelines (City of Hope IRB Protocol 11276). The biopsy specimens were immediately frozen in optimal cutting temperature media on dry ice, and transferred to the City of Hope Translational Research Laboratory before processing. Sections of mouse xenografts and the human tumor biopsies were imaged on a Zeiss LSM 510 inverted confocal scanning microscope (PlanApochormat ×63/1.4 oil objective; Zeiss).

ACKNOWLEDGMENTS. We thank Alasdair McDowall [Director of the electron microscopy facility in the Jensen laboratory at the California Institute of Technology (Caltech)] for his help in obtaining the cryo-TEM images. The work at Caltech was financially supported by National Cancer Institute Grant CA 151819. The electron microscopy facility in the Jensen laboratory at California Institute of Technology is supported in part by the Gordon and Betty Moore Foundation, the Agouron Institute, and the Beckman Foundation at Caltech.

1. Davis ME, Chen ZG, Shin DM (2008) Nanoparticle therapeutics: An emerging treatment modality for cancer. *Nat Rev Drug Discov* 7(9):771–782.
2. Petros RA, DeSimone JM (2010) Strategies in the design of nanoparticles for therapeutic applications. *Nat Rev Drug Discov* 9(8):615–627.
3. Shi J, Xiao Z, Kamaly N, Farokhzad OC (2011) Self-assembled targeted nanoparticles: Evolution of technologies and bench to bedside translation. *Acc Chem Res* 44(10): 1123–1134.
4. Sheridan C (2012) Proof of concept for next-generation nanoparticle drugs in humans. *Nat Biotechnol* 30(6):471–473.
5. Bourzac K (2012) Nanotechnology: Carrying drugs. *Nature* 491(7425):S58–S60.
6. Bouchie A (2012) Companies in footrace to deliver RNAi. *Nat Biotechnol* 30(12):1154–1157.
7. Weiss GJ, et al. (2013) First-in-human phase 1/2a trial of CRLX101, a cyclodextrin-containing polymer-camptothecin nanopharmaceutical in patients with advanced solid tumor malignancies. *Invest New Drugs* 31(4):986–1000.
8. Hrkach J, et al. (2012) Preclinical development and clinical translation of a PSMA-targeted docetaxel nanoparticle with a differentiated pharmacological profile. *Sci Transl Med* 4(128):128ra39.
9. Davis ME, et al. (2010) Evidence of RNAi in humans from systemically administered siRNA via targeted nanoparticles. *Nature* 464(7291):1067–1070.
10. Cheng Z, Al Zaki A, Hui JZ, Muzykantov VR, Tsourkas A (2012) Multifunctional nanoparticles: Cost versus benefit of adding targeting and imaging capabilities. *Science* 338(6109):903–910.
11. Oerlemans C, et al. (2010) Polymeric micelles in anticancer therapy: Targeting, imaging and triggered release. *Pharm Res* 27(12):2569–2589.
12. Davis ME (2009) Design and development of IT-101, a cyclodextrin-containing polymer conjugate of camptothecin. *Adv Drug Deliv Rev* 61(13):1189–1192.
13. Schluep T, et al. (2009) Pharmacokinetics and tumor dynamics of the nanoparticle IT-101 from PET imaging and tumor histological measurements. *Proc Natl Acad Sci USA* 106(27):11394–11399.
14. Schluep T, Cheng J, Khin KT, Davis ME (2006) Pharmacokinetics and biodistribution of the camptothecin-polymer conjugate IT-101 in rats and tumor-bearing mice. *Cancer Chemother Pharmacol* 57(5):654–662.
15. Gaur S, et al. (2012) Preclinical study of the cyclodextrin-polymer conjugate of camptothecin CRLX101 for the treatment of gastric cancer. *Nanomedicine* 8(5):721–730.
16. Numbenjapon T, et al. (2009) Preclinical results of camptothecin-polymer conjugate (IT-101) in multiple human lymphoma xenograft models. *Clin Cancer Res* 15(13): 4365–4373.
17. Schluep T, et al. (2006) Preclinical efficacy of the camptothecin-polymer conjugate IT-101 in multiple cancer models. *Clin Cancer Res* 12(5):1606–1614.
18. Cheng J, Khin KT, Jensen GS, Liu A, Davis ME (2003) Synthesis of linear, beta-cyclodextrin-based polymers and their camptothecin conjugates. *Bioconjug Chem* 14(5):1007–1017.
19. Mi Z, Burke TG (1994) Marked interspecies variations concerning the interactions of camptothecin with serum albumins: A frequency-domain fluorescence spectroscopic study. *Biochemistry* 33(42):12540–12545.
20. Li B, et al. (2005) Butyrylcholinesterase, paraoxonase, and albumin esterase, but not carboxylesterase, are present in human plasma. *Biochem Pharmacol* 70(11):1673–1684.
21. Cabral H, et al. (2011) Accumulation of sub-100 nm polymeric micelles in poorly permeable tumours depends on size. *Nat Nanotechnol* 6(12):815–823.
22. Xiao K, et al. (2011) The effect of surface charge on *in vivo* biodistribution of PEG-oligocholic acid based micellar nanoparticles. *Biomaterials* 32(13):3435–3446.
23. Szebeni J, et al. (2002) Role of complement activation in hypersensitivity reactions to Doxil and Hynic PEG liposomes: Experimental and clinical studies. *J Liposome Res* 12(1-2):165–172.
24. Uziely B, et al. (1995) Liposomal doxorubicin: Antitumor activity and unique toxicities during two complementary phase I studies. *J Clin Oncol* 13(7):1777–1785.
25. Gabizon A, et al. (2008) An open-label study to evaluate dose and cycle dependence of the pharmacokinetics of pegylated liposomal doxorubicin. *Cancer Chemother Pharmacol* 61(4):695–702.
26. Song G, Wu H, Yoshino K, Zamboni WC (2012) Factors affecting the pharmacokinetics and pharmacodynamics of liposomal drugs. *J Liposome Res* 22(3):177–192.
27. Caron WP, Song G, Kumar P, Rawal S, Zamboni WC (2012) Interpatient pharmacokinetic and pharmacodynamic variability of carrier-mediated anticancer agents. *Clin Pharmacol Ther* 91(5):802–812.
28. Hamaguchi T, et al. (2010) Phase I study of NK012, a novel SN-38-incorporating micellar nanoparticle, in adult patients with solid tumors. *Clin Cancer Res* 16(20):5058–5066.
29. Lim WT, et al. (2010) Phase I pharmacokinetic study of a weekly liposomal paclitaxel formulation (Genexol-PM) in patients with solid tumors. *Ann Oncol* 21(2):382–388.
30. Burke TG, Mi Z (1994) The structural basis of camptothecin interactions with human serum albumin: impact on drug stability. *J Med Chem* 37(1):40–46.
31. Kurono Y, Miyajima M, Ikeda K (1993) [Interaction of camptothecin derivatives with human plasma proteins *in vitro*.]. *Yakugaku Zasshi* 113(2):167–175, Japanese.
32. Conover CD, Greenwald RB, Pendri A, Gilbert CW, Shum KL (1998) Camptothecin delivery systems: Enhanced efficacy and tumor accumulation of camptothecin following its conjugation to polyethylene glycol via a glycine linker. *Cancer Chemother Pharmacol* 42(5):407–414.
33. Rowinsky EK, et al. (2003) A phase I and pharmacokinetic study of pegylated camptothecin as a 1-hour infusion every 3 weeks in patients with advanced solid malignancies. *J Clin Oncol* 21(1):148–157.
34. Posey JA, 3rd, et al. (2005) Phase 1 study of weekly polyethylene glycol-camptothecin in patients with advanced solid tumors and lymphomas. *Clin Cancer Res* 11(21):7866–7871.
35. Schoemaker NE, et al. (2002) A phase I and pharmacokinetic study of MAG-CPT, a water-soluble polymer conjugate of camptothecin. *Br J Cancer* 87(6):608–614.
36. Wachters FM, et al. (2004) A phase I study with MAG-camptothecin intravenously administered weekly for 3 weeks in a 4-week cycle in adult patients with solid tumours. *Br J Cancer* 90(12):2261–2267.
37. Koizumi F, et al. (2006) Novel SN-38-incorporating polymeric micelles, NK012, eradicate vascular endothelial growth factor-secreting bulky tumors. *Cancer Res* 66(20):10048–10056.
38. Sapra P, et al. (2008) Novel delivery of SN38 markedly inhibits tumor growth in xenografts, including a camptothecin-11-refractory model. *Clin Cancer Res* 14(6):1888–1896.
39. Kurzrock R, et al. (2012) Safety, pharmacokinetics, and activity of EZN-2208, a novel conjugate of polyethylene glycol and SN38, in patients with advanced malignancies. *Cancer* 118(24):6144–6151.